Analysing of Electromagnetic Coupling Effects of Cables in Protective Small-Room of Substation Based on the Random Coupling Model

Jie-Qing Fan[1, *], Yao Li[1], and Ying Pan[2]

Abstract—The electromagnetic circumstance of the small-room of substation turns to be more complex with the increase of the voltage level of the power grid. In this paper, a physical model for protective small-room of substation on the basis of the random plane wave hypothesis and wave-chaotic approach is constructed to get the scattering parameters, combining the Random Coupling Model (RCM) to deduce inducted voltage of coaxial cable terminal and making statistical analysis and prediction for electromagnetic quantity coupled to the cable terminal. The results of simulation by FEKO show the validity of the method introduced in this paper, which provides guidance for the electromagnetic protection in the protective small-room.

1. INTRODUCTION

Protective small-room is widely used in substations in China, where amount of secondary equipment is located and interfered by electromagnetic interference. In order to reduce the effect of the electromagnetic interference, substation protective small-rooms are always designed as enclosed spaces which are made of galvanized steel. In practice, in the walls of a small-room, lots of apertures in different sizes and different shapes are perforated to meet the demands of maintenance, cooling, observation, etc. In addition, appropriate channels are needed to provide spaces for cables of the power supply system, signal transmission systems, control systems, etc. All of these approaches provide "back door" through which the electromagnetic interference signals can couple into the protective small-room [1].

Small-rooms can be considered as lossy wave chaotic cavities by comparing those sizes and the wavelength of electromagnetic interference [4]. There are numerous types of electromagnetic interference towards protective small-room including high frequency interference [2]. Among those, two of them are prominent which cannot be ignored. One is generated by the communication transmitter which is used in substations with frequency range from $27 \sim 590\,\text{MHz}$ [2, 3], and the other is generated by GIS's switching operation with the frequency up to $300\,\text{MHz}$. Meanwhile, the typical volume of a protective small-room is usually over several hundred of m^3. Hence small-rooms can be considered as an electrically large object. Furthermore, the internal field distributions of protective small-rooms caused by electromagnetic interference are usually extremely sensitive to those inner complex structures, where the secondary equipment with a number of cables is located.

A method called RCM which can describe the statistical properties of coupling electromagnetic quantity at target point of complex cavities based on plane wave hypothesis and wave-chaotic approach was put forward by Zheng et al. [4], and its applicability was verified by experimental method by Hemmady et al. [5]. To analyze system-level electromagnetic coupling effect of two computer boxes

[1] College of Electrical and Electronic Engineering, North China Electrical Power University, Beijing, China. [2] Aostar Information Technologies Co., Ltd., China.

connected by a coaxial cable, the method combining RCM and BLT is improved by Xin et al. [6]. Furthermore, the method is applied to analyze the prediction of induced voltages on ports in a single-chamber and a double-chamber in three-dimensional complex enclosures with apertures by Gil et al. [7] and Fan et al. [8], respectively. The magnitudes of RF fields on electrically large components within a complex 3-D enclosure were experimentally analyzed by Zachary et al. [9]. The radiation efficiency of the antenna is used to modify RCM's impedance description in the case of lossy port in the complex cavity by Bisrat et al. [10]. RCM was further extended aiming at the case of an active nonlinear circuit added to the ray-chaotic 1/4-bowtie cavity by Min et al. [11], and RCM was integrated inside the Kron's formalism by Chaouki et al. [12]. The RCM method was improved by using Time Gate Method to get the loss parameter by Addissie et al. [13, 14]. In the case of an electrically narrow aperture in cavity walls, Gabriele et al. formulated and investigated the RCM [15]. Refs. [16] and [17] imported RCM into the fields of wireless communication channel analyzing and sonas' signal focusing in Ray-Chaotic Enclosure by Gabriele et al. and Bo et al., respectively. However, the works above are all focused on coupling electromagnetic quantity in the common metal enclosures with the volume of enclosures far less than $1\,\mathrm{m}^3$ irradiated by the interference signal with high frequency (usually greater than $3\,\mathrm{GHz}$).

The primary interest in this paper is to introduce the RCM to the prediction of the coupling electromagnetic quantity in the protective small-rooms. For this purpose, the protective small-rooms are regarded as a lossy wave chaotic metal shielding enclosure with cables placed in it which can be considered as the target of electromagnetic interference, and a physical model for protective small-room of substation based on random plane wave hypothesis and wave-chaotic approach is proposed. Then, S parameters of a protective small-room are obtained by FEKO, which are used to solve the coupling electromagnetic quantity based on RCM. At last, the influences of interference signal parameters are analyzed, such as pulse width, rising time, and pulse number.

2. SOLUTION OF TARGET POINT INDUCED VOLTAGE BASED ON RCM

As depicted in Figure 1, we consider the protective small-room of a typical $500\,\mathrm{kV}$ substation of China power grid as the reference model ($10\,\mathrm{m} \times 8.5\,\mathrm{m} \times 4.3\,\mathrm{m}$), which is an electrically large regular rectangular enclosure with plenty of apertures in its walls, through which the complex electromagnetic interference can couple into the inside of the enclosure. Hence, the apertures are treated as ports in this paper. A Cartesian coordinate system is established, shown as in Figure 1, where o is the origin of the coordinates, and the length, width, and height of the cavity are $10\,\mathrm{m}$, $8.5\,\mathrm{m}$, and $4.3\,\mathrm{m}$, which are parallel to the x-axis, y-axis, and z-axis, respectively. There exist N ports named as "port 1" to "port N", which represent the N apertures in the protective small-room walls, respectively. A coaxial cable is mounted in the cavity and seems as the target point ("port p") shown as the thick black line in Figure 1, then the induced electromagnetic quantity on this point is calculated.
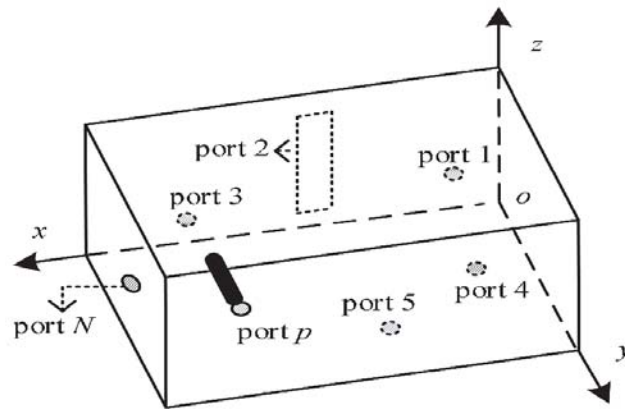
Figure 1. Model of induced voltage of coaxial cable terminal in the protective small-room in substation of China.

As shown in Figure 1, we treat the ith port $(1 \leq i \leq N)$ as the excitation current sources with a vector I, then the electromotive force V between port N and target point p can be gained, shown as follows

$$\mathbf{V} = \mathbf{ZI} \tag{1}$$

where $\mathbf{Z}$ is the impedance matrix between the excitation source and target point, which can be expressed as

$$\mathbf{Z} = -\frac{j}{\pi} \sum_{n=1}^{N} \Delta k \frac{\left(\text{Re}\left\{\mathbf{Z}^{\text{rad}}\right\}\right)^{1/2} w_n w_n^T \left(\text{Re}\left\{\mathbf{Z}^{\text{rad}}\right\}\right)^{1/2}}{k^2 - k_n^2} \tag{2}$$

where k is the wave number of the electromagnetic interference signal; the term k_n^2 is defined as a matrix eigenvalue of the Gaussian Orthogonal Ensemble (GOE) or the Gaussian Unitary Ensemble (GUE) matrix eigenvalues; and there is $k_{m+1} \geq k_m$. k satisfies $k^2 = \omega^2/c^2$, where ω is the angular frequency of the excitation signal. The quantity Δk represents the mean-spacing between the eigenvalues of the cavity; w_n is an M-dimensional vector, representing the mode of port coupling the electromagnetic signal; and $\mathbf{Z}^{\text{rad}}$ is a radiation impedance of the cavity, which can be expressed as

$$\mathbf{Z}^{\text{rad}} = \text{Re}\left\{\mathbf{Z}^{\text{rad}}\right\} + j\text{Im}\left\{\mathbf{Z}^{\text{rad}}\right\} \tag{3}$$

In particular, the impedance matrix $\mathbf{Z}$ gives rise to large fluctuations according to $k^2 \to k_n^2$, which can be divided into two parts $\mathbf{Z} = \bar{\mathbf{Z}} + \tilde{\mathbf{Z}}$. $\bar{\mathbf{Z}}$ is the steady part (mean value of $\mathbf{Z}$), and $\tilde{\mathbf{Z}}$ is the fluctuating part, then it can be written as follows

$$\bar{\mathbf{Z}} = -\frac{j}{\pi} \sum_{n=1}^{N} \Delta k \cdot E\left\{ \frac{\left(\text{Re}\left\{\mathbf{Z}^{\text{rad}}\right\}\right)^{1/2} w_n w_n^T \left(\text{Re}\left\{\mathbf{Z}^{\text{rad}}\right\}\right)^{1/2}}{k^2 - k_n^2} \right\} \tag{4}$$

And

$$\tilde{\mathbf{Z}} = \mathbf{Z} - \bar{\mathbf{Z}} = j\left(\text{Re}\left\{\mathbf{Z}^{\text{rad}}\right\}\right)^{1/2} \mathbf{Z}\text{norm}\left(\text{Re}\left\{\mathbf{Z}^{\text{rad}}\right\}\right)^{1/2} \tag{5}$$

where $\mathbf{Z}$norm is the normalized impedance of the cavity and is written as

$$\mathbf{Z}\text{norm} = \frac{-1}{\pi} \sum_{n=1}^{N} \frac{w_n w_n^T}{k^2 - k_n^2} = -\frac{j}{\pi} \mathbf{W} \frac{1}{\lambda - j\alpha\mathbf{I}} \mathbf{W}^T \tag{6}$$

α is the loss factor matrix of the cavity, and its element $\alpha_{ip} = \frac{1}{\pi\sigma_{Z_{\text{normip}}}^2}$ represents the loss of cavity from port i to port p. Meanwhile, $\mathbf{W}$ is the coupling matrix that represents the coupling of excitation aperture and intrinsic modes of the cavity, whose elements satisfy the independent Gaussian distribution with zero mean, and unit variance. λ is the diagonal matrix, whose elements satisfy the Wigner semicircle distribution [4], and $\mathbf{I}$ is the unit matrix. The cavity impedance matrix is given by

$$\mathbf{Z} = j\left\{ \text{Im}\left\{\mathbf{Z}^{\text{rad}}\right\} + \left(\text{Re}\left\{\mathbf{Z}^{\text{rad}}\right\}\right)^{1/2} \mathbf{Z}\text{norm}\left(\text{Re}\left\{\mathbf{Z}^{\text{rad}}\right\}\right)^{1/2} \right\} \tag{7}$$

To simplify the analysis, we consider Z_0 as the characteristic impedance of the cavity with $Z_0^{=}50\,\Omega$ and also introduce radiation impedance $\mathbf{Z}^{\text{rad}} = Z_0^{1/2}(\mathbf{I}+\mathbf{S}^{\text{rad}})(\mathbf{I}-\mathbf{S}^{\text{rad}})^{-1}Z_0^{1/2}$, where $\mathbf{S}^{\text{rad}}$ is a radiation scattering parameters of the cavity. When a large number of cavity scattering parameters $\mathbf{S}$ are averaged, their mean values are closely parallel to their radiation scattering parameters, that is $\mathbf{S}^{\text{rad}} = \langle\mathbf{S}\rangle_n = \mathbf{S}^{\text{avg}}$ $(n \geq 200)$, which can be obtained by experimental measurements or by numerical simulation. Similarly, the cavity radiation impedance can be rewritten as $\mathbf{Z}^{\text{rad}} = \langle\mathbf{Z}\rangle_n = \mathbf{Z}^{\text{avg}}$. Furthermore, taking non-ubiquitous short traces trajectories effect into account [4], the impedance can be rewritten as

$$\mathbf{Z}^{\text{avg}} = j\left\{ \text{Im}\left\{\mathbf{Z}^{\text{avg}}\right\} + (\text{Re}\left\{\mathbf{Z}^{\text{avg}}\right\})^{1/2} \mathbf{Z}\text{norm}(\text{Re}\left\{\mathbf{Z}^{\text{avg}}\right\})^{1/2} \right\} \tag{8}$$

Hence, the normalized impedance matrix of cavity can be expressed as

$$\mathbf{Z}\text{norm} = (\text{Re}\left\{\mathbf{Z}^{\text{avg}}\right\})^{-1/2} (\mathbf{Z} - j\text{Im}\left\{\mathbf{Z}^{\text{avg}}\right\}) (\text{Re}\left\{\mathbf{Z}^{\text{avg}}\right\})^{-1/2} \tag{9}$$

Then, we can generate the normalized impedance ofa protective small-room by the Monte Carlo method based on the RCM model, and it can be expressed as

$$\mathbf{Z}_{\text{norm}}^{\text{RCM}} = \begin{bmatrix} \text{Re}\left(z_{\text{norm11}}^{\text{RCM}}\right) + j\text{Im}\left(z_{\text{norm11}}^{\text{RCM}}\right) & \ldots & \text{Re}\left(z_{\text{norm1N}}^{\text{RCM}}\right) + j\text{Im}\left(z_{\text{norm1N}}^{\text{RCM}}\right) \\ \ldots & \ldots & \ldots \\ \text{Re}\left(z_{\text{normN1}}^{\text{RCM}}\right) + j\text{Im}\left(z_{\text{normN1}}^{\text{RCM}}\right) & \ldots & \text{Re}\left(z_{\text{normNN}}^{\text{RCM}}\right) + j\text{Im}\left(z_{\text{normNN}}^{\text{RCM}}\right) \end{bmatrix} \tag{10}$$

where both $\text{Re}\left(z_{\text{normjj}}^{\text{RCM}}\right)$ and $\text{Im}\left(z_{\text{normjj}}^{\text{RCM}}\right)$ are $N(1, \frac{1}{\pi\alpha_{jj}})$ when $i = j \in \{1, 2, 3, \ldots, N\}$; and both $\text{Re}\left(z_{\text{normij}}^{\text{RCM}}\right)$ and $\text{Im}\left(z_{\text{normij}}^{\text{RCM}}\right)$ are $N(0, \frac{1}{\pi\alpha_{ij}})$ when $i, j \in \{1, 2, 3, \ldots, N\}, i \neq j$. $N(x, y)$ represents a Gaussian distribution with x mean and y variance when $\alpha \gg 1$ [7]. The impedance of cavity based on the RCM theory can be expressed as

$$\mathbf{Z}^{\text{RCM}} = j\left\{\text{Im}\{\mathbf{Z}^{\text{avg}}\} + (\text{Re}\{\mathbf{Z}^{\text{avg}}\})^{1/2}\,\mathbf{Z}_{\text{norm}}^{\text{RCM}}\,(\text{Re}\{\mathbf{Z}^{\text{avg}}\})^{1/2}\right\} \tag{11}$$

As suggested above, when the scattering parameters of cavity ($\mathbf{S}$) are obtained by simulation, the impedance of cavity $\mathbf{Z}^{\text{RCM}}$ can be calculated by Equations (7)–(11) based on the RCM. Supposing that the $\mathbf{i}$th port is a planar aperture through which the excitation source is accessed from the outside, we can define the power of excitation source as $P(f)$. Thus the induced voltage of coaxial cable terminal at the target point (port p) can be expressed as Equation (12) with the RCM methods.

$$\left|V_{ip}^{\text{RCM}}\right| = \left|\sqrt{\frac{2P(f)\left|Z_{ip}^{\text{RCM}}\right|^2}{\left|Z_{ii}^{\text{RCM}}\right|}}\right| \tag{12}$$

This paper has adopted a method of reverberation chamber to meet the complex internal structure characteristics of the protective small-room of substation and utilized FEKO to obtain the scattering parameters $\mathbf{S}$ of cavity.

3. EXTRACTION SIMULATION MODEL BY S PARAMETERS

3.1. Establishment of Simulation Model

As shown in Figure 2, the reverberation chamber founded in FEKO is identical to the model of Figure 1 which is equipped with a regular rectangle cavity, a stirrer, a transmit antenna, and a coaxial cable
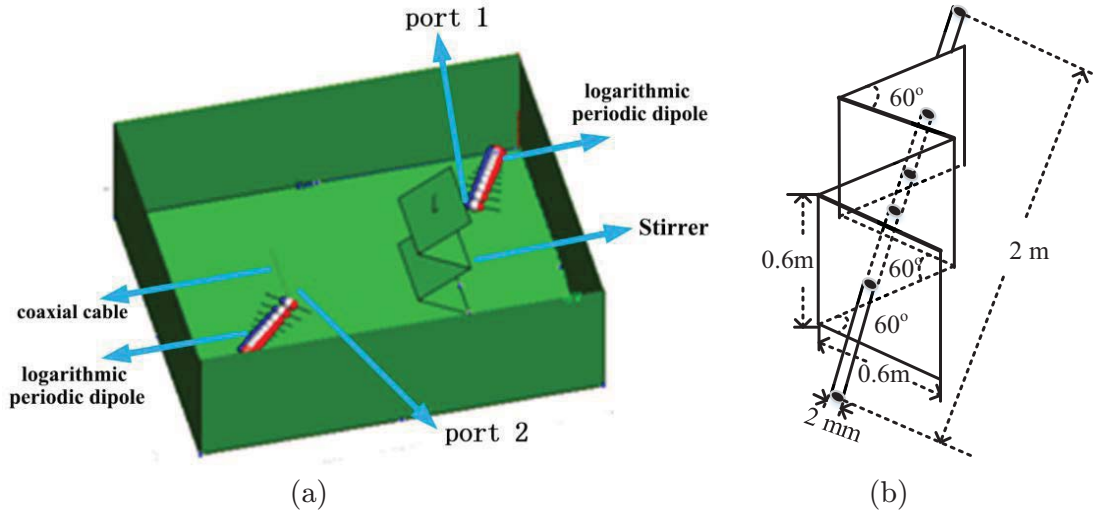
Figure 2. The profile of the reverberation room model. (a) the reverberation room model of the protective small-room of substation modeled in FEKO; (b) the size of the stirrer.

ended with resistances. Galvanized steel is selected as the materials of cavity and stirrer (thickness 1 mm, conductivity $\sigma = 1.69 \times 10^7$ S/m, relative permeability $\mu_r = 1$, and magnetic loss factor $\tan \delta_u = 0.0$). A stirrer composed of a metal cylinder and 4 metal square plates is used to create the situation of wave chaotic, which is parallel to the wall of cavity located at a distance of more than a quarter of the interference signal wavelength λ from the wall. The size of the stirrer is shown as in Figure 2(b). The transmitting antenna is selected by a logarithmic periodic dipole, arrayed with frequency spectra from 160 MHz to 300 MHz, which is regarded as the excitation port "port 1". The logarithmic periodic dipole used to radiate electromagnetic wave has serval antenna elements. Among the elements, the shortest one is 0.5 mm; the longest is 1.022 mm; the shortest spacing is 0.094 mm; the longest spacing is 0.167 mm; the growth factor is 0.8667; the power of excitation source on the antenna is set to 100 W; and the voltage is 10 V. The coaxial cable is selected as RG58C/U owned in FEKO, which is internally mounted 2 meters above the bottom of the cavity, and a 50 Ω load is used to connect the cable to the cavity at each of the antenna. The coaxial cable terminal, near the end of the antenna, is regarded as the target point (port 2).

3.2. Simulation of S Parameters and Coaxial Cable Terminal Induced Voltage Calculation

As shown in Figure 3, under the precondition of setting frequency spectra from 200 MHz to 220 MHz with the frequency step 0.2 MHz, we control the stirrer to rotate every 5 degrees for 4 rounds by MATLAB programming to construct 288 kinds of different small-room internal field structures of the substation, by which we can simulate the scattering parameters of the cavity $\mathbf{S}$. Ultimately, the terminal induced voltage of the coaxial cables can be obtained.
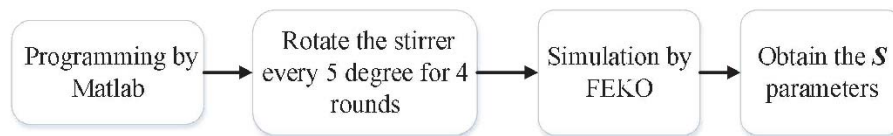
Figure 3. Schematic diagram of the S parameters obtained.

4. RESULTS AND DISCUSSION

4.1. Validity Verification of the Proposed Method

As described in Section 3, a large ensemble of coaxial cable terminating voltage and its Probability Density Function (PDF) can be obtained based on RCM and by the simulation directly. We analyze electromagnetic waves ranging from 200 MHz to 220 MHz, and its wavelength is smaller than the cavity size, which meets the requirements of RCM applications [4, 5]. As shown in Figure 4, there is a good agreement between the simulation and RCM-predicted induced voltage PDFs for the coaxial cable terminal, which proves the validity of the RCM in predicting and analyzing coupling electromagnetic at target points of the protective small-room in substation.

4.2. Prediction of Induced Voltage at Target Points Motivated by Gaussian Pulse Based on RCM

Combining the frequency spectra and the form of the high frequency interference signal that frequently threatens the protective small-room of substation, we take the modulated Gaussian pulse with the frequency range from 200 MHz to 220 MHz as the excitation source to analyze and forecast the induced electromagnetic at target points. The expression of the modulated Gaussian pulse signal is as follows

$$u(t) = U_0 \exp[-4\pi(t - t_0)^2/\tau^2] \sin(2\pi f t) \tag{13}$$

where U_0 is the pulse amplitude, f the carrier frequency, τ the pulse width, and t_0 the peak time. Setting t_r as the rising edge time of the Gaussian pulse, which represents the time, it takes for the amplitude to rise from 10% to 90% of U_0.
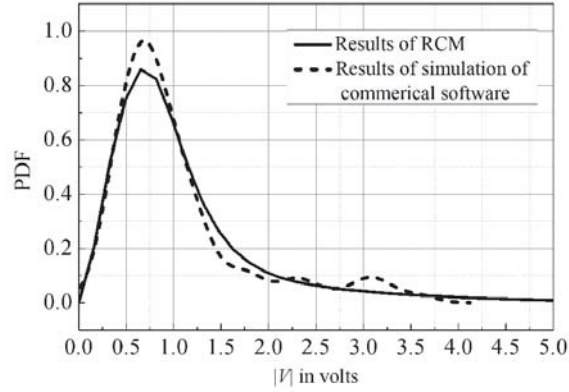
Figure 4. Comparison of RCM-predicted and simulated the coaxial cable terminal induced voltage PDFs.

When the excitation source is Gaussian pulse multi-pulses, its expression can be rewritten as follows

$$u(t) = U_0 \sin(2\pi f t) \sum_{n=1}^{N} \exp[-4\pi(t - t_0 - (n-1)t_p)^2/\tau^2] \tag{14}$$

where t_p is the pulse interval, n the number of pulses, and the other parameters are the same as in Equation (13).

4.3. Establishment of Simulation Model

After the text edit has been completed, the paper is ready for the template. Duplicate the template file by using the Save As command, and use the naming convention prescribed by your conference for the name of your paper. In this newly created file, highlight all of the contents and import the text file you prepared. You are now ready to style your paper; use the scroll down window on the left of the MS Word Formatting toolbar.

4.3.1. Prediction of Induced Voltage at Target Points Irradiated by Gaussian Pulse With Different Pulse Widths, Rising Edges and Pulse Amplitude

To investigate the effect of different pulse parameters, we firstly assign $U_0 = 1\,\text{kV/m}$, $f = 210\,\text{MHz}$, and $t_0 = 0.8\tau$, then explore the change of induced voltage at target points with different pulse widths $2\,\text{ns}$, $4\,\text{ns}$, $6\,\text{ns}$, $8\,\text{ns}$, and $10\,\text{ns}$, respectively. The results are given in Figure 5(a) and Figure 5(b), which represent the influence on PDF of induced voltage and the maximum induced voltage values at target points, respectively.

Secondly, we explore the influence of pulse rising edge on the induced voltage at the target port with different $t_r 1\,\text{ns}$, $2\,\text{ns}$, $3\,\text{ns}$, $4\,\text{ns}$, and $5\,\text{ns}$, respectively. The results are shown in Figure 6(a) and Figure 6(b), which represent the influence on PDF of induced voltage and the maximum induced voltage values at target points, respectively.

Finally, we set the pulse amplitude as $1\,\text{kV}$, $2\,\text{kV}$, $3\,\text{kV}$, $4\,\text{kV}$, and $5\,\text{kV}$, respectively, the pulse width τ is $1\,\text{ns}$, and the other parameters remain unchanged. Therefore, the changes of induced voltage at target points with different pulse amplitude can be investigated. The results are shown in Figure 7(a) and Figure 7(b), which represent the influence on PDF of induced voltage and its maximal induced voltage values at target points, respectively.

It can be seen from Figure 5(a), Figure 6(a), and Figure 7(a) that the PDF curves of the induced voltage at target points become spreading to the higher voltage direction with the increases of the Gaussian pulse width, the rising edge, and the amplitude, which mean increasing the probability of the higher induced voltage. Meanwhile, the level of the induced voltage rises nonlinearly (seen from Figure 5(b) and Figure 6(b)) with the increase of the width and rising edge of the pulse, and almost rises linearly (seen from Figure 7(b)) with the increase of the pulse amplitude. It can be explained that

(a)

(b)
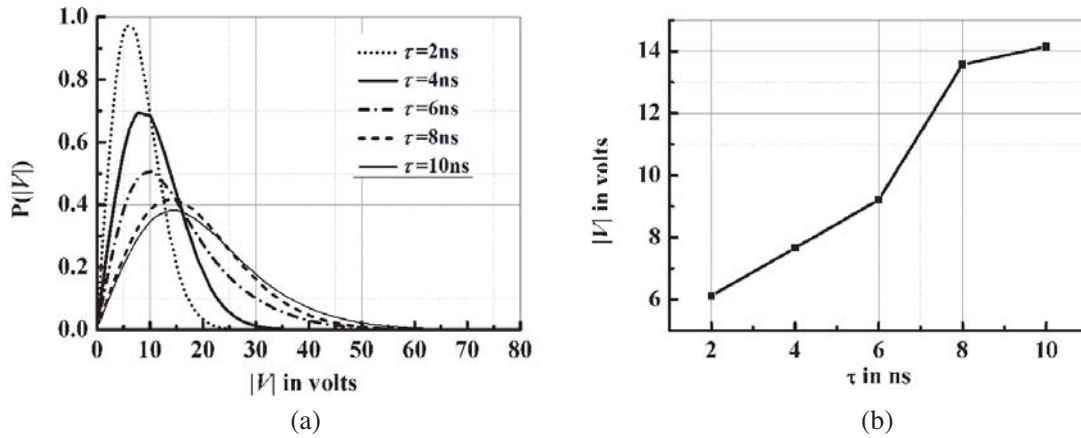
Figure 5. Curves of PDFs induced voltage at target points (a) vary with the pulse width τ; (b) vary with the pulse width τ.

(a)

(b)
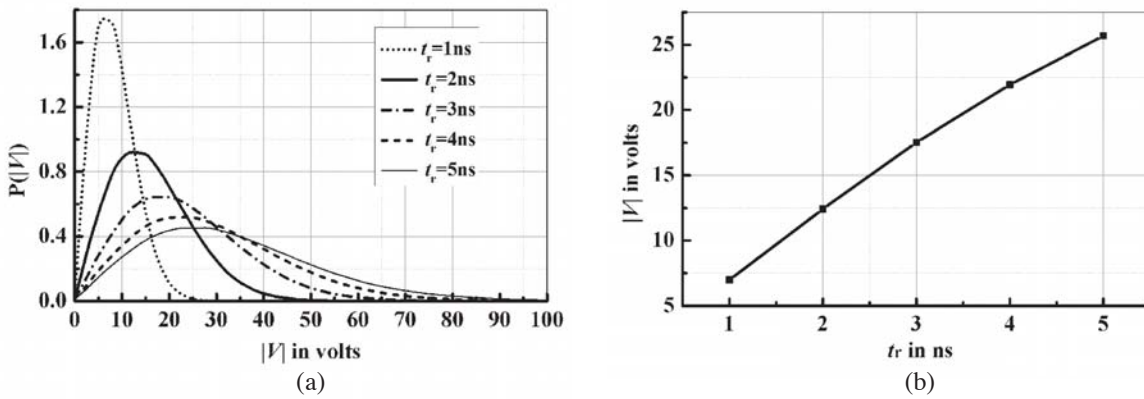
Figure 6. Curves of (a) PDFs induced voltage at target points vares with the pulse rising edge t_r; (b) the peak of PDFs induced voltage at target points varies with the pulse rising edge t_r.

(a)

(b)
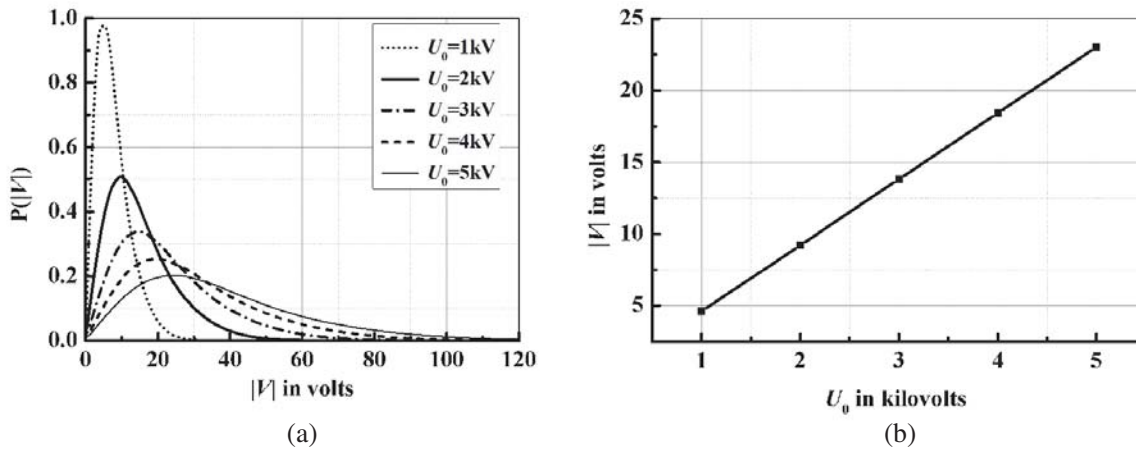
Figure 7. Curves of (a) PDFs induced voltage at target points varies with the pulse amplitude U_0; (b) the peak of PDFs induced voltage at target points varies with the pulse amplitude U_0.

with wider pulse width, the pulse rising edge and lager pulse amplitude will lead to more energy of the pulse, then the induced voltage at the target port will increase because of the cumulative effect of the coupling electromagnetic energy, and it will increase the probability of the higher voltage and raise the level of the induced voltage.

4.3.2. Prediction of Induced Voltage at the Target Point Motivated by Gaussian Multi-Pulse with Different Interval of Pulse and Different Number of Pulse

In this section, we investigate the impact of the interval and number of the Gaussian pulses on the damage probability for the electronic device. Firstly, we normalize the pulse energy by numerical integration as follows

$$\int_{-\infty}^{+\infty} u^2(t)dt = \mathrm{E} \tag{15}$$

where E is the total energy of normalized pulse. When $U_0 = 1\,\mathrm{kV/m}$, $\tau = 1\,\mathrm{ns}$, $f = 210\,\mathrm{MHz}$, $t_0 = 0.8\tau$, $n = 1$, the normalized gross energy E can be calculated by Eq. (14), and the result is $E = 2.613 \times 10^{-3}\,\mathrm{J}$. Then the impact of the interval and the number of the Gaussian pulse on the induced voltage at the target point can be obtained under under the condition of the constant Gaussian multi-pulse energy E.

When $n = 5$, the changes of induced voltage at target points can be explored with different pulse intervals t_p 1.2 ns, 1.4 ns, 1.6 ns, 1.8 ns, and 2.0 ns, respectively. The results are shown in Figure 8(a) and Figure 8(b), which represent the influence on PDF of induced voltage and the induced voltage values at target points, respectively.
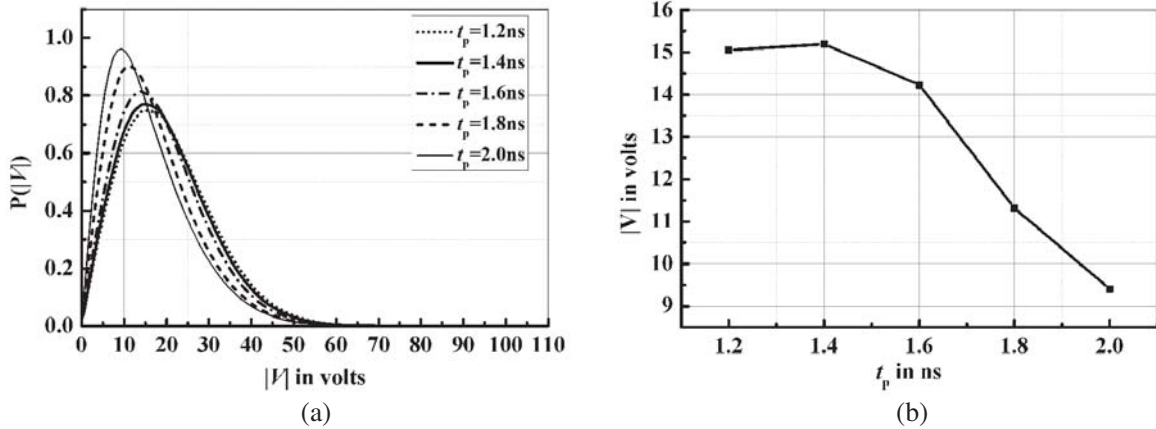
Figure 8. Curves of (a) PDFs induced voltage at target points vary with the pulse interval t_p; (b) the peak of PDFs induced voltage at target points vary with the pulse interval t_p.

Then, t_p is set as an invariable with 1 ns, and pulse number n varies from 1 to 5, respectively. The changes of induced voltage at target points with different pulse numbers can be explored. The results are reported in Figure 9(a) and Figure 9(b), which represent the influence on PDF of induced voltage and its maximum induced voltage values at target points, respectively.

It can be seen from Figure 8(a) and Figure 9(a) that when the total energy of Gaussian multi-pulse is fixed, the PDF curves of the induced voltage at the target point become spreading to the direction of higher voltage with the decrease of the Gaussian pulse interval and the increase of the Gaussian pulse number. It means that the level of the induced voltage rises (see Figure 8(b) and Figure 9(b)). The results can be regarded as that when the total energy is fixed, (1) the influence on the induced voltage of the multi-pulse is more significant than single pulse, which can be explained as that although the amplitude of the multi-pulses is lower than that of single pulse, the induced electromagnetic quantity caused by multi-pulses will last longer, then the cumulative effect of the coupling electromagnetic energy if more significantly; (2) when the intervals between the multi-pulses decrease, the next pulse
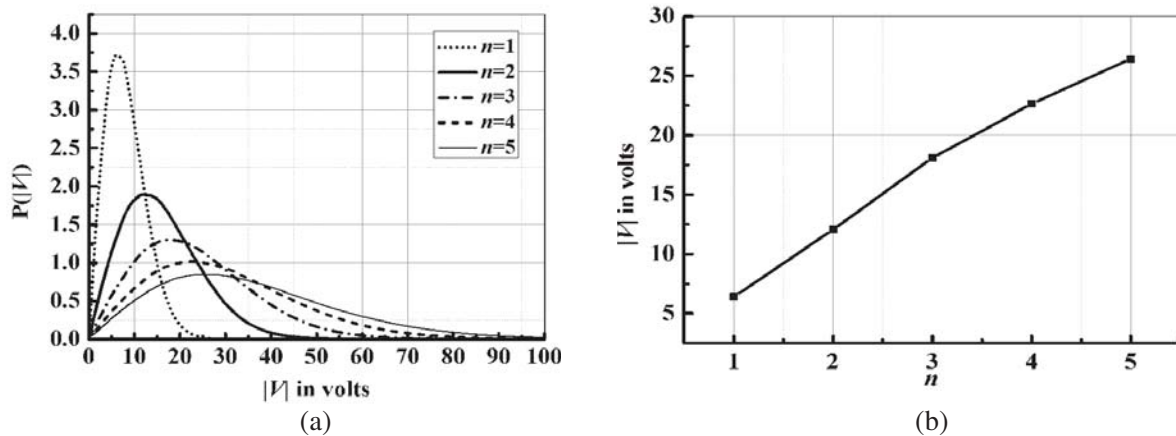
Figure 9. Curves of (a) PDFs induced voltage at target points vary with the pulse number n; (b) the peak of PDFs induced voltage at target points vary with the pulse number n.

works before the effect of the last pulse decays sufficiently, so the strong cumulative effect of induced electromagnetic quantity appears at the target point, which leads to the increase of the level of induced voltage; (3) when the intervals of the multi-pulses increase, the effect of the last pulse has been decayed sufficiently before the next pulse starts to work, so the cumulative effect is not obvious, and the induced voltage at the target point will keep at a relatively low level.

In conclusion, the research has benefited from the prediction of RCM, which can always be used to evaluate the objective induced voltage of other types of interfering signals quickly in the same frequency spectra, thus greatly improving the efficiency to such solution, reducing the cost, and providing a way of guiding the work for electromagnetic protection.

5. CONCLUSIONS

The study of the electromagnetic interference coupling to secondary equipment in protective small-rooms of substation is of great interest in the field of electromagnetic compatibility engineering, especially with the complication of UHV power grid and the electromagnetic environment. This thesis applies RCM to predict and analyze the quantity of EMI coupling to targeted coaxial cable terminal within protective small-room of substation, and shows the validity of this method through a series of model simulation and data analysis, which provides an idea of the electromagnetic protection for a protective small-room. However, the measured data are insufficient with the limit of the experimental conditions, so the verification of this method remains to be further studied.

ACKNOWLEDGMENT

REFERENCES

1. Zhen, G. L., "Coupling path analysis of electromagnetic disturbances in a substation," *High Voltage Engineering*, Vol. 34, No. 11, 2423–2427, 2008.
2. Guang, Z. Z., L. Yao, Q. W. Bao, X. W. Zhang, and X. Wu, "Research on shielding measurement of 100kV substation protective chamber in switch yard," *High Voltage Engineering*, Vol. 32, No. 12, 62–88, 2006.
3. Wiggins, C. M. and S. E. Wright, "Switching transient fields in substation," *IEEE Trans on Power Delivery*, Vol. 6, No. 2, 591–600, 1991.

4. Zheng, X., J. T. M. Antonsen, and E. Ott, "Statistics of impedance and scattering matrices of chaotic microwave cavities with multiple ports," *Electromagnetics*, Vol. 26, No. 1, 37–55, 2006.

5. Hemmady, S., T. M. Antonsen, E. Ott, and S. M. Anlage, "Statistical prediction and measurement of induced voltages on components within complicated enclosures: A wave-chaotic approach," *IEEE Trans. on Electromagnetic Compatibility*, Vol. 54, No. 4, 758–771, 2012.

6. Xin, L., C. Meng, Y. N. Liu, E. Schamiloglu, and S. Hemmady, "Experimental verification of a stochastic topology approach for high-power microwave effects," *IEEE Transactions on Electronic Compatibility*, Vol. 57, No. 3, 1–6, 2015.

7. Gil, J. G., Z. B. Drikas, T. D. Andreadis, and S. M. Anlage, "Prediction of induced voltages on ports in complex, three-dimensional enclosures with apertures, using the random coupling model," *IEEE Trans on Electromagnetic Compatibility*, Vol. 58, No. 5, 1535–1540, 2016.

8. Fan, J. Q., Y. Pan, and J. H. Hao, "Application of the random coupling model to electromagnetic coupling effect analysis of complex double cavity," *Progress In Electromagnetics Research Letters*, Vol. 65, 81–87, 2017.

9. Zachary, B. D., G. G. Jesus, K. H. Sun, D. A. Tim, Y. Jen-Hao, T. T. Biniyam, and S. M. Anlage, "Application of the random coupling model to electromagnetic statistics in complex enclosures," *IEEE Trans. Electromag. Compat.*, Vol. 56, No. 6, 1480–1487, 2014.

10. Bisrat, D. A., C. R. John, and M. A. Thomas, "Application of the Random Coupling Model to Lossy Ports in Complex Enclosures," *IEEE Metrology for Aerospace (MetroAeroSpace) Conference*, 214–219, Benevento, Italy, Jun. 2015.

11. Min, Z., O. Edward, M. A. Thomas, and S. M. Anlage, "Nonlinear wave chaos: statistics of second harmonic fields," *Chaos*, Vol. 27, 103114, 2017.

12. Chaouki, K., M. Olivier, G. Gabriele, T. J. Antonsen, E. Otto, and S. M. Anlage, "Stochastic Kron's model inspired from the random coupling model," *2015 IEEE International Symposium on Electromagnetic Compatibility (EMC)*, 935–940, Dresden Germany, Aug. 2015,

13. Addissie, B. D., J. C. Rodgers, and T. M. Antonsen, "Extraction of the coupling impedance in overmoded cavities," *Wave Motion.*, 0165–2125, 2018.

14. Addissie, B. D., J. C. Rodgers, and T. M. Antonsen, "Application of the random coupling model to lossy ports in complex enclosures," *2015 IEEE Metrology for Aerospace (Metro Aero Space)*, Benevento, Italy, Jun. 4–5, 2015.

15. Gabriele, G., M. A. Thomas, M. A. Steven, and E. Ott, "A statistical model for the excitation of cavities through apertures," *IEEE Trans. Electromag. Compat.*, Vol. 57, No. 5, 1049–1061, 2015.

16. Gabriele, G., C. Xiaoming, and M. A. Thomas, "Random coupling model for wireless communication channels," *2014 International Symposium on Electromagnetic Compatibility (EMC Europe)*, 878–882, Gothenburg, Sweden, Sept. 2014.

17. Bo, X., M. A. Thomas, O. Edward, and S. M. Anlage, "Focusing waves at an arbitrary location in a ray-chaotic enclosure using time-reversed synthetic sonas," *Phys. Rev. E*, Vol. 93, 052205, 2016.